6 Diagrammatic Monte Carlo for the Hubbard Model

Riccardo Rossi
Institute of Physics
École Polytechnique Fédérale de Lausanne (EPFL)
Route Cantonale, 1015 Lausanne, Switzerland

Contents

E. Pavarini and E. Koch (eds.)
Correlated Materials: Methods and Applications
Modeling and Simulation Vol. 16, Forschungszentrum Jülich, 2026
ISBN 978-3-95806-909-1 http://www.cond-mat.de/events/correl26

1 Introduction

The main obstacle to a reliable determination of the properties of an interacting quantum many-body system is the exponential scaling of the Hilbert space with system size. The thermodynamic properties of a macroscopic system do not change when considering a system with a few additional particles, yet the computational cost of the direct exact solution increases many times. This means that the exponential cost of the exact solution is not justified by an intrinsic exponential complexity of the thermodynamic problem, and that most of the exponentially-large wave function does not lead to any observable physical effect.
Diagrammatic Monte Carlo avoids this exponential scaling issue by directly evaluating physical observables, which are typically few-body correlation functions. This is done by writing an expansion in terms of "connected" correlations, which have a well-defined thermodynamic limit. Loosely speaking, in many situations a moderate number of connected correlations is able to combinatorially generate the exponential amount of information contained in the wave function, at least for few-body observables.
We emphasize here the distinction between standard perturbative approaches and diagrammatic Monte Carlo. In conventional perturbation theory, one typically selects a limited subset of diagrams, which may then be resummed to infinite order. This approach can be effective for weakly correlated systems, or in special cases where a particular class of diagrams dominates. In diagrammatic Monte Carlo, by contrast, all diagrammatic contributions to a given expansion are sampled up to a chosen order, without distinguishing between different classes of diagrams, except for the hierarchy imposed by the choice of expansion itself. The convergence, or lack thereof, is then assessed by comparing results obtained at different truncation orders, providing a systematic way to control the reliability of the final result.
We also want to stress the difference with respect to other quantum Monte Carlo techniques, which can also be used to compute the expectation value of observables as the ratio of two partition-function-like objects

$$\langle O \rangle = \frac{A}{Z}\,, \tag{1}$$

where A and Z are the exponential of extensive quantities, $A, Z \sim e^{\#\text{Volume}/\text{Temperature}}$. Typical quantum Monte Carlo approaches sample both A and Z, which results generically, for fermionic systems, in an exponential scaling with system size and temperature, a fact known as the sign problem, which has its origin in the fact that A and Z are exponentially-large quantities. In diagrammatic Monte Carlo, instead, one writes expansions of the form

$$\langle O \rangle = O_0 + O_1 + O_2 + \dots\,, \tag{2}$$

where each of the O_j coefficients is an intensive, or at most extensive, quantity. This means that the fermionic sign problem cannot apply by definition, and we can take the thermodynamic limit directly. By contrast, cancellations in the calculation of O_j are instead welcomed, as this just means that the contribution of the O_j term is smaller. In this document we review that, for fermionic systems, there are indeed such strong cancellations between different Feynman

diagrams that the resulting series has a non-zero radius of convergence, in contrast to what happens for bosonic theories, which have generically zero radius of convergence. This fact is important from a theoretical point of view as it allows one to show that fermionic systems on the lattice can be simulated on a classical computer with polynomial complexity, at least in some regions of the phase diagram.

Document organization. The purpose of this document is to present an introduction to the techniques that are used for diagrammatic Monte Carlo calculations in the Hubbard model. The method consists of three main parts or tasks involving our central object, the expansion:

1. **Choosing the expansion: diagrammatic renormalization and beyond (Sec. 3)**. Choosing the right expansion for the problem studied is crucial. For the expectation value of a physical observable, O_{phys}, we write

$$O_{\text{phys}} = O_{\text{expan}}(z{=}1), \tag{3}$$

   where z is some effective coupling constant, and where we have introduced the expansion function $O_{\text{expan}}(z)$, which has a $z{=}0$ Taylor expansion of the form

$$O_{\text{expan}}(z) = \sum_{n=0}^{N} z^n \; O_{\text{expan},n} + \mathcal{O}(z^{N+1}). \tag{4}$$

   The expansion function $O_{\text{expan}}(z)$ is completely arbitrary and in general unphysical apart from $z{=}1$.

   We are going to review that fully-self-consistent one-particle renormalization expansions can converge to a wrong physical answer. It turns out that the naive bare expansion and non-diagrammatic schemes based on the general formalism of shifted-actions are instead particularly effective and safe choices.

2. **Computing the expansion: summing all diagrams to high orders (Sec. 4)**. Next, we need to discuss the evaluation of the coefficients of the expansion, $O_{\text{expan},n}$, which can be written as a sum of Feynman diagrams.

   We mentioned the fact that there are strong cancellations between fermionic diagrams, which means that diagram enumeration is highly inefficient. We are going to describe techniques that make it possible to sum exactly over *all* Feynman-diagram topologies, for various expansions and physical quantities. As we show that computing the sum of all Feynman diagrams at fixed expansion order is NP-hard, the best we can reasonably achieve in general are exponential-in-order algorithms, which are still a massive improvement from the factorially-scaling enumeration technique.

   Once all the diagrams of the expansion are summed over, it remains to perform an integration over the internal variables, which can be handled with a specifically-designed Markov-chain Monte Carlo procedure over sets of variables.

3. **Summing the expansion: convergence, singularities and resummation (Sec. 5).** The cancellation between the factorial number of diagrams for fermionic systems on a lattice is almost perfect, resulting in a finite radius of convergence at non-zero temperature.

   When the radius of convergence is larger than one, the naive truncated sum of the z-expansion evaluated at $z{=}1$ gives an exponentially-convergent result. As the computational cost scales exponentially with order, this results in a polynomial-time algorithm.

   When the radius of convergence is smaller than one, we know that there is a singularity somewhere at $|z|{<}1$. This singularity is determined by the physical properties of the system and it can be approximately identified with a calculation done at large-enough orders. If there is a singularity in the segment $z{\in}[0,1]$, this corresponds to a physical phase transition, which means that the expansion is unable to enter that particular phase and another expansion should be used. If there is no indication of a singularity for $z{\in}[0,1]$, analytical continuation to the physical point $z{=}1$ is, in principle, possible, and we discuss techniques to achieve this, which are sometimes referred to as "resummation". The consistency of the procedure is then checked also by comparing the results at different expansion orders and for various resummation techniques.

2 Notation and theoretical setup

The Hubbard model. In this document we consider the Hubbard model. However, the formalism and the discussions presented here generalize in a straightforward way to any lattice system. For continuous-space or long-range systems, after a more careful analysis of the applicable expansions, most considerations presented in this document still apply.
We work at thermal equilibrium at inverse temperature β. The Hubbard model [1–3] is defined by the grand-canonical Hamiltonian

$$\hat{H}_{\text{phys}} = -\mu \sum_{\sigma,\boldsymbol{r}} \hat{n}_\sigma(\boldsymbol{r}) - \sum_{\sigma,\boldsymbol{r},\boldsymbol{r}'} t_{\boldsymbol{r},\boldsymbol{r}'}\, \hat{c}^\dagger_\sigma(\boldsymbol{r}) \hat{c}_\sigma(\boldsymbol{r}') + U \sum_{\boldsymbol{r}} \hat{n}_\uparrow(\boldsymbol{r})\, \hat{n}_\downarrow(\boldsymbol{r}), \tag{5}$$

where $\sigma \in \{\downarrow,\uparrow\}$ denotes a spin index, $\boldsymbol{r}$ a lattice coordinate, $\hat{c}_\sigma(\boldsymbol{r})$ $\left(\hat{c}^\dagger_\sigma(\boldsymbol{r})\right)$ the fermionic annihilation (creation) operators, $\hat{n}_\sigma(\boldsymbol{r}) = \hat{c}^\dagger_\sigma(\boldsymbol{r})\hat{c}_\sigma(\boldsymbol{r})$, μ the chemical potential, t the hopping matrix, U the onsite Coulomb repulsion, and "phys" means that we are interested in a fixed, given, physical value of the Hubbard-model parameters μ, t and U.

The partition function and the grand potential. From the grand-canonical Hamiltonian $\hat{H}$, we introduce the grand-canonical partition function

$$Z = \operatorname{Tr} e^{-\beta \hat{H}_{\text{phys}}}. \tag{6}$$

The partition function is the *exponential* of an extensive quantity.
In order to obtain an extensive quantity, we take the logarithm of the partition function, which gives the grand potential Ω

$$\Omega_{\text{phys}} = -\frac{1}{\beta} \log Z, \tag{7}$$

where "phys" hereafter is used to mean the physical value of the quantity in the Hubbard model at fixed chemical potential μ and interaction strength U. We stress that this notation is useful to avoid confusion when introducing expansion functions

$$\Omega_{\text{phys}} = \Omega_{\text{expan}}(z{=}1), \tag{8}$$

where z is an effective coupling constant and $\Omega_{\text{expan}}(z)$ is an expansion function, several examples of which will be given later in the document.

Imaginary-time formalism and notation for spacetime and collective variables. For the theoretical description of the thermal properties of a quantum system, it is convenient to use the imaginary-time formalism. For simplicity, we set the value of the reduced Planck constant $\hbar$ to one. We denote by capital roman letters like $X = (\boldsymbol{r}, \tau)$ spacetime variables consisting of a lattice position $\boldsymbol{r}$ and an imaginary time $\tau \in [0, \beta]$. We use calligraphic capital roman letters like $\mathcal{X} = (\boldsymbol{r}, \tau, \sigma)$ for spin-spacetime collective coordinates, where $\sigma \in \{\uparrow, \downarrow\}$. We also use shorthand integration symbols

$$\int dX\, f(X) = \int_0^\beta d\tau \sum_{\boldsymbol{r}} f(\boldsymbol{r}, \tau)\ , \qquad \int d\mathcal{X}\, f(\mathcal{X}) = \int_0^\beta d\tau \sum_{\boldsymbol{r},\sigma} f(\boldsymbol{r}, \tau, \sigma). \tag{9}$$

For an operator $\hat{O}$, we define the imaginary-time Heisenberg picture as

$$\hat{O}(\tau) = e^{\tau \hat{H}_{\text{phys}}}\ \hat{O}\ e^{-\tau \hat{H}_{\text{phys}}}. \tag{10}$$

Green function. Using the time-ordered operation $\hat{T}$, which orders Heisenberg-picture fermionic operators in terms of the imaginary-time coordinate, we define the Green function as

$$G_{\text{phys};\mathcal{Y},\mathcal{Y}'} = -\frac{1}{Z}\,\text{Tr}\left[\ e^{-\beta \hat{H}_{\text{phys}}}\ \hat{T}\left(\hat{c}(\mathcal{Y})\hat{c}^\dagger(\mathcal{Y}')\right)\right]. \tag{11}$$

The $U{=}0$ value of the Green function defines the physical non-interacting Green function of the Hubbard model

$$G_{0;\text{phys}} = G_{\text{phys}}\big|_{U=0}. \tag{12}$$

Functional integral formalism. We review here the standard Grassmann-valued functional integration technique for fermions, which is useful to derive diagrammatic identities and for renormalization. The action of the Hubbard model can be written in the form

$$S_{\text{phys}} = -\int d\mathcal{X}\, d\mathcal{Y}\ \bar{\varphi}(\mathcal{X})\, G^{-1}_{0;\text{phys}}(\mathcal{X}, \mathcal{Y})\, \varphi(\mathcal{Y}) + U \int dX\, (\bar{\varphi}_\uparrow \bar{\varphi}_\downarrow \varphi_\downarrow \varphi_\uparrow)(X), \tag{13}$$

where $\varphi(\mathcal{X})$ and $\bar{\varphi}(\mathcal{X})$ are Grassmann fields, and where $G_{0;\text{phys}}$ is the non-interacting Green function of the Hubbard model (see Eq. (12)). It is convenient to use a shorthand notation for the kinetic part of the action

$$\int d\mathcal{X}\, d\mathcal{Y}\ \bar{\varphi}(\mathcal{X})\, G^{-1}_{0;\text{phys}}(\mathcal{X}, \mathcal{Y})\, \varphi(\mathcal{Y}) = \langle \varphi | G^{-1}_{0;\text{phys}} | \varphi \rangle. \tag{14}$$

The functional integral formalism is useful as it avoids the use of quantum operators and of the time-ordering operation. For instance, the grand potential corresponds to a "simple" integral over Grassmann fields

$$\Omega_{\text{phys}} = -\frac{1}{\beta} \log \int \mathcal{D}[\varphi, \bar{\varphi}] \; e^{-S_{\text{phys}}}. \tag{15}$$

More generally, we can write any time-ordered correlation function as an expectation value over the Grassmann-valued path-integral measure $\mathcal{D}[\varphi, \bar{\varphi}] \; e^{-S_{\text{phys}}}$.

3 Choosing the expansion: Diagrammatic renormalization and beyond

In this document, we use a purely-functional formalism to describe renormalization. The advantages with respect to the standard diagrammatic formalism are: (i) it provides a clearer view of the assumptions made in the renormalization procedure; (ii) it provides more efficient ways to perform renormalization; (iii) it can be used to build non-diagrammatic renormalization procedures. Some of the functional expansions we consider in this document have a natural diagrammatic interpretation, which we briefly mention.

At the center of this algebraic formulation stand bare-expansion functionals, discussed in Sec. 3.1. Bare-expansion functionals are not only used to define the bare expansion, but, most importantly, they are also used to define renormalization.

A general formalism for renormalization, which can be applied to traditional diagrammatic expansions and beyond, is based on so-called shifted actions (see Sec. 3.2 and Ref. [4, 5]). Some applications are discussed, in particular the study of broken-symmetry phases and the full renormalization of the chemical potential.

Finally, as a cautionary tale on the dangers of a cavalier attitude in renormalization, in Sec. 3.3 we discuss the issue of the misleading convergence of the popular fully-self-consistent one-particle renormalization, which has been shown to happen in the Hubbard model at strong-enough coupling. This is due to the non-invertibility of the mapping between the non-interacting Green function and the interacting one, and shows up, in the shifted-action, as an unphysical singularity, an artifact of the renormalization scheme that does not correspond to a physical phase transition. This shows that the choice of the expansion is crucial: careful attention should be devoted not only to optimizing convergence, but also to guaranteeing that the convergent result corresponds to the physical one. We also discuss a large class of renormalization procedures that do not suffer from the misleading convergence found in the full one-particle renormalization, and which can therefore be safely used without conditions.

3.1 Bare-expansion functionals

3.1.1 The bare-expansion action functional

We define the bare-expansion action functional S_{bare} as

$$S_{\text{bare}}[G_0, V] := -\langle\varphi|G_0^{-1}|\varphi\rangle + \int dX\ V(X)\ (\bar{\varphi}_\uparrow\bar{\varphi}_\downarrow\varphi_\downarrow\varphi_\uparrow)(X), \tag{16}$$

which is a generalization of S_{phys} introduced in Eq. (13) where we have added, for later use, a spacetime-dependent onsite interaction $V(X)$.

3.1.2 Retrieving the physical action from the bare-expansion action

The most important property of the bare action S_{bare} is that it can reproduce the physical Hubbard-model action S_{phys} (defined in Eq. (13)) when the non-interacting Green function G_0 is equal to the physical Hubbard-model Green function $G_{0;\text{phys}}$ (see Eq. (12) for a definition) and when the interaction $V(X)$ is uniform and equal to the Hubbard U parameter (introduced in Eq. (5))

$$S_{\text{bare}}\big[G_0{=}G_{0;\text{phys}}, V(X){=}U\big] = S_{\text{phys}}. \tag{17}$$

3.1.3 Bare-expansion functionals for other quantities

Partition function. Using S_{bare}, we can define any other bare-expansion functionals by using the Grassmann functional integral. The bare-expansion functional for the zero-interaction-normalized partition function, $\tilde{Z}_{\text{bare}}$, is

$$\tilde{Z}_{\text{bare}}[G_0, V] := \frac{\int D[\bar{\varphi},\varphi]\ e^{-S_{\text{bare}}[G_0,V]}}{\int D[\bar{\varphi},\varphi]\ e^{-S_{\text{bare}}[G_0,0]}}\,. \tag{18}$$

Grand potential. The bare-expansion grand-potential functional Ω_{bare} is similarly defined as

$$\Omega_{\text{bare}}[G_0, V] - \Omega_{\text{bare}}[G_0, 0] := -\frac{1}{\beta}\log\tilde{Z}_{\text{bare}}[G_0, V]. \tag{19}$$

Green function. The bare-expansion functional for the Green function, G_{bare}, is defined as

$$G_{\text{bare};\mathcal{Y},\mathcal{Y}'}[G_0, V] = -\frac{\int D[\bar{\varphi},\varphi]\ e^{-S_{\text{bare}}[G_0,V]}\ \varphi(\mathcal{Y})\bar{\varphi}(\mathcal{Y}')}{\int D[\bar{\varphi},\varphi]\ e^{-S_{\text{bare}}[G_0,V]}} = \frac{A_{\text{bare};\mathcal{Y},\mathcal{Y}'}[G_0, V]}{\tilde{Z}_{\text{bare}}[G_0, V]}\,, \tag{20}$$

where we have introduced the auxiliary quantity $A_{\text{bare};\mathcal{Y},\mathcal{Y}'}[G_0, V]{=}-\frac{\int D[\bar{\varphi},\varphi]\ e^{-S_{\text{bare}}[G_0,V]}\ \varphi(\mathcal{Y})\bar{\varphi}(\mathcal{Y}')}{\int D[\bar{\varphi},\varphi]\ e^{-S_{\text{bare}}[G_0,0]}}$.

Self-energy. When $G_{\text{bare};\mathcal{Y},\mathcal{Y}'}[G_0, V]$ is viewed as a function of $\mathcal{Y}$ and $\mathcal{Y}'$, it is a formally invertible operator, and we denote its inverse by $G^{-1}_{\text{bare};\mathcal{Y},\mathcal{Y}'}[G_0, V]$. The bare-expansion self-energy functional Σ_{bare} is defined as

$$\Sigma_{\text{bare}}[G_0, V] = G_0^{-1} - G^{-1}_{\text{bare}}[G_0, V]. \tag{21}$$

3.2 Shifted-action expansions

3.2.1 General formalism for fermionic renormalization

The bare-expansion functionals, defined in Sec. 3.1, form the basis of the shifted-action formalism for renormalization.

Shifted action. The most general fermionic renormalization scheme can be obtained by a z-dependent *shifted action* $S_{\text{expan}}(z)$

$$S_{\text{expan}}(z) := S_{\text{bare}}\big[G_0(z), V(X){=}z\,U\big], \tag{22}$$

where $V(X) = z\,U$ is uniform in spacetime and proportional to the Hubbard-model U, and where $G_0(z)$ is any function of z with the property

$$G_0(z{=}1) = G_{0;\text{phys}}. \tag{23}$$

Retrieving the physical action. The shifted-action definition immediately implies

$$S_{\text{expan}}(z{=}1) = S_{\text{phys}}. \tag{24}$$

Retrieving physical quantities. The definition of the shifted action is such that any quantity computed with the $S_{\text{expan}}(z)$ action, by construction, coincides with the physical one when the coupling constant z is equal to one, $z{=}1$. As an explicit example, consider the shifted-action Green function

$$G_{\text{expan}}(z) = -\frac{\int D[\bar\varphi,\varphi]\; e^{-S_{\text{expan}}(z)}\;\varphi(\mathcal{Y})\bar\varphi(\mathcal{Y}')}{\int D[\bar\varphi,\varphi]\; e^{-S_{\text{expan}}(z)}} = G_{\text{bare}}\big[G_0(z), V(X){=}z\,U\big]. \tag{25}$$

Thanks to Eq. (24), we immediately obtain $G_{\text{expan}}(z{=}1) = G_{\text{phys}}$.

Expansion coefficients. The expansion coefficients are defined from the Taylor expansion in z

$$G_{\text{expan}}(z) = G_{\text{bare}}\big[G_0(z), V(X){=}z\,U\big] = \sum_{n=0}^{N} z^n\, G_{\text{expan},n} + \mathcal{O}(z^{N+1}). \tag{26}$$

3.2.2 The bare expansion

The bare expansion is simply obtained by considering a shifted action where the non-interacting Green function is a constant function of the coupling constant z: $G_0(z) = G_{0;\text{phys}}$

$$S_{\text{bare-ex}}(z) := S_{\text{bare}}\big[G_{0;\text{phys}}, V(X){=}z\,U\big]. \tag{27}$$

For instance, the bare expansion function for the grand potential is

$$\Omega_{\text{bare-ex}}(z) := \Omega_{\text{bare}}\big[G_{0;\text{phys}}, V(X){=}z\,U\big]. \tag{28}$$

3.2.3 Linearly-shifted actions I: the α-shift expansion

In this document we discuss some of the choices of shifted actions that are relevant for the Hubbard model. The simplest type of shifted action is just a linear function of z.

From the shifted Hamiltonian to the shifted action. The minimal choice for a linear function is just a chemical potential shift, which is operationally referred to as "α-shift", and can be defined by the shifted Hamiltonian

$$\hat{H}_{\alpha\text{-sh}}(z) = \hat{H}_{\text{phys}} + (1-z)\,\alpha\,U \sum_{\boldsymbol{r},\sigma} \hat{n}_\sigma(\boldsymbol{r}) - (1-z)\,U \sum_{\boldsymbol{r}} \hat{n}_\uparrow(\boldsymbol{r})\hat{n}_\downarrow(\boldsymbol{r}), \tag{29}$$

where $\alpha \in \mathbb{R}$ is a free parameter.
We note that the $z{=}0$ shifted Hamiltonian, $\hat{H}_{\alpha\text{-sh}}(z{=}0)$, is quadratic. This means that the corresponding shifted-action $S_{\alpha\text{-sh}}(z)$ is also quadratic for $z{=}0$, and can therefore be written in the form of Eq. (22) with $G_0^{-1}(z) = G_{01}^{-1} + z\,\Sigma_{01}$, for some G_{01} and Σ_{01}.

Freedom in the shifted action. We also note the following important property

$$\hat{H}_{\alpha\text{-sh}}(z{=}1) \equiv \hat{H}_{\text{phys}}, \tag{30}$$

which means that the associated shifted action satisfies the same property: $S_{\alpha\text{-sh}}(z{=}1) = S_{\text{phys}}$. The α-shift expansion coefficients depend on α, but the final result of the expansion, when evaluated for $z{=}1$, must be α-independent.

Diagrammatic interpretation. The α-shift expansion corresponds to a linear renormalization of the chemical potential as a function of the effective interaction strength $z\,U$. The appearance of such a linear term can be justified by the fact that the mean-field choice $\alpha = n_0/2$, where n_0 is the non-interacting spin-σ density, cancels the first-order (aka Hartree) contribution to the particle number, and eliminates all "tadpole" diagrams from the expansion.

3.2.4 Linearly-shifted actions II: symmetry breaking terms

Breaking the symmetry in the expansion. A bare expansion cannot converge in a symmetry-broken phase as the corresponding order parameter is trivially zero at all orders. To study these phases, we must consider an expansion starting point that breaks the symmetry [6,7]. In analogy with mean-field theory, this can be achieved in a straightforward way within the linear shifted-action formalism.

Example: an antiferromagnetic phase expansion. To be concrete, let us consider the case of the antiferromagnetic phase in the Hubbard model on a bipartite lattice made of sublattices A and B. We introduce

$$v_\sigma(\boldsymbol{r}) = \alpha\,U + \gamma\,U\,s_\sigma(\boldsymbol{r}), \tag{31}$$

where $\alpha, \gamma \in \mathbb{R}$ are free parameters, $\sigma \in \{\downarrow, \uparrow\}$ and $s_\uparrow(\boldsymbol{r})=1$ for $\boldsymbol{r} \in A$, $s_\uparrow(\boldsymbol{r})=-1$ otherwise, and $s_\downarrow(\boldsymbol{r})=-s_\uparrow(\boldsymbol{r})$. The shifted Hamiltonian is

$$\hat{H}_{\alpha\gamma\text{-sh}}(z) = \hat{H}_{\text{phys}} + (1-z)\sum_{\boldsymbol{r},\sigma} v_\sigma(\boldsymbol{r})\,\hat{n}_\sigma(\boldsymbol{r}) - (1-z)\,U\sum_{\boldsymbol{r}} \hat{n}_\uparrow(\boldsymbol{r})\hat{n}_\downarrow(\boldsymbol{r}). \tag{32}$$

where $\hat{H}_{\alpha\gamma\text{-sh}}(z=0)$ is quadratic, and the choice of the local potentials $v_\sigma(\boldsymbol{r})$ guarantees that $\hat{H}_{\alpha\gamma\text{-sh}}(z=1) = \hat{H}_{\text{phys}}$. This means that we can retrieve the physical answer by evaluating the expansion function at $z=1$. If this procedure is performed in the infinite-system-size limit, one can effectively compute quantities in the antiferromagnetic phase of the original physical Hubbard model.

We also note that the linear shifted-action formalism for symmetry breaking can be straightforwardly extended to superfluid phases using the Nambu formalism. We can also consider adding non-linear symmetry-breaking terms, which can be particularly useful if there is no mean-field theory that breaks that symmetry.

3.2.5 Linearly-shifted actions III: bosonic shifts

A straightforward way to treat renormalization beyond the one-particle channel is to use Hubbard-Stratonovich fields to decompose the Hubbard interaction.

Example: particle-particle channel renormalization. To illustrate this procedure, we focus on the particle-particle channel. We can rewrite the physical-system action in terms of the "bosonic" field $\eta(X)$

$$S_{\text{expan}}(z) = -\langle\varphi|G_0^{-1}(z)|\varphi\rangle - \int_{X,Y} \bar{\eta}(X)\eta(Y)W_0^{-1}(X,Y)(z) + \sqrt{z}\int_X \big(\bar{\eta}\varphi_\uparrow\varphi_\downarrow + c.c.\big)(X). \tag{33}$$

If $G_0(z=1) = G_{0;\text{phys}}$ and $W_0^{-1}(X,Y)(z=1) = \delta(X,Y)/U$, then $S_{\text{expan}}(z=1) = S_{\text{phys}}$.

If $W_0(z)$ is not a constant function of z, the shifted action formalism effectively achieves a renormalization in the particle-particle channel. For instance, if we consider the linear shifted-action choice

$$W_0^{-1}(z) = \Gamma_0^{-1} + z\Pi_0, \tag{34}$$

where Γ_0 is the sum of all particle-particle bubble diagrams, and Π_0 is the particle-particle bubble, then this shifted-action expansion is equivalent to a diagrammatic expansion in which all particle-particle bubble diagrams are eliminated. There is a corresponding functional definition of this expansion in terms of the elimination of the first term in the expansion of the particle-particle vertex. This particle-particle-renormalized expansion can be generalized to higher orders and to various degrees of self-consistency.

3.3 Why full one-particle renormalization can converge to the wrong answer

The shifted-action formalism is very general, and can describe general diagrammatic and non-diagrammatic expansion schemes with various degrees of self-consistency. As we briefly describe here, fully-self-consistent schemes, while powerful and physically motivated, can, in some situations, artificially create unphysical singularities in the shifted action that are not associated with physical phase transitions, which lead in some cases to a misleading convergence towards an incorrect unphysical result (see Ref. [8]). This means that they should be used with care. Their applicability to a given situation can be checked by using the following sufficient criterion: if we are strictly inside the radius of convergence for the shifted action when viewed as a function of the coupling constant z, then a misleading convergence to an unphysical result can be ruled out.

Here, we limit the discussion to two expansions: (i) the full renormalization of the chemical potential to fix the density, which does not present any such issues and can always be used without checking any applicability condition; (ii) the full one-particle renormalization, whose shifted-action has unphysical branches that make the renormalized expansion converge to a wrong result at strong coupling.

3.3.1 Fully-self-consistent expansions I: full chemical-potential renormalization

As a generalization of the α-shift expansion above, we can consider the problem of finding the chemical potential $\mu(z)$ such that the density $n(z)$ is a constant function of the coupling constant z

$$\mu(z) \qquad \text{such that} \qquad n(z) = n. \tag{35}$$

This expansion, while working in the grand-canonical ensemble where the number of particles is not fixed, shares features with the canonical ensemble. It is useful, in particular, to disentangle the trivial density-changing effect of the change of the coupling constant z from genuine interaction effects. We emphasize that this expansion, despite its simple functional definition, has no diagrammatic interpretation.

The parametrization $\mu(z)$ does not typically create unphysical singularities: for all $z \in [0, 1]$, $\mu(z)$ is a real chemical potential of some physical Hubbard model, and a singularity in the mapping $\mu \to n$ would mean a physical phase transition involving an incompressible phase of matter at that particular density and interaction strength.

3.3.2 Fully-self-consistent expansions II: one-particle renormalization and misleading convergence

Extending the logic of the full chemical-potential renormalization introduced above, we can consider a non-interacting z-dependent Green function $G_0(z)$ that makes the interacting Green function $G(z)$ a z-independent function

$$G_0(z) \qquad \text{such that} \qquad G(z) = G. \tag{36}$$

This expansion is often referred to as the one-particle bold(-line) expansion, where the "bold" terminology comes from its Feynman-diagram interpretation, where self-energy diagram insertions can be replaced by a bold line representing the sum of all such insertions.

Functional definition. We now introduce the bold expansion more carefully by considering the full V-potential dependence. We consider the self-consistency condition for the non-interacting "bold" Green function $G_{0;\text{bold}}[G,V]$, which is a functional of the Green function G and the spacetime-dependent interaction $V(X)$, defined such that the interacting Green function G is independent of the interaction strength field V

$$G^{-1} = \big(G_{0;\text{bold}}[G,V]\big)^{-1} - \Sigma_{\text{bare}}\big[G_{0;\text{bold}}[G,V],V\big]. \tag{37}$$

It is also useful to express the self-energy directly in terms of the interacting Green function by introducing the self-energy bold functional $\Sigma_{\text{bold}}[G,V]$

$$\Sigma_{\text{bold}}[G,V] := \Sigma_{\text{bare}}\big[G_{0;\text{bold}}[G,V],V\big], \tag{38}$$

where $G_{0;\text{bold}}[G,V]$ is a solution of the self-consistent Eq. (37). The functional formalism we have used here is fully non-perturbative.

Perturbative bold functionals. When the self-consistent equation for the bold formalism is solved order-by-order in powers of V, the coefficients of the Σ_{bold} expansion can be interpreted in terms of so-called skeleton Feynman diagrams, i.e., diagrams that cannot be made disconnected after removing one or two G lines.

The perturbative solution for $G_{0;\text{bold}}[G,V]$ need not be the unique solution of the non-linear equation: importantly, this non-uniqueness is the basis of a crucial issue that we now discuss. The non-invertibility of the mapping creates singularities, and, most importantly, these singularities do not allow the analytic continuation of the perturbative branch to the physical point. This general mathematical fact is understood already at the level of a simple toy model introduced in Ref. [9], a zero-dimensional version of the Hubbard model, whose Green function is

$$G_{\text{bare}}(G_0,V) = \frac{G_0}{1 - V\,G_0^2}. \tag{39}$$

The relation $G_0 \to G$ is not one-to-one: this creates a singularity in bold functionals. For instance, the self-energy bold functional is

$$\Sigma_{\text{bold}}(G,V) = \frac{-1 \pm \sqrt{1+4\,VG^2}}{2G}, \tag{40}$$

where the $+$ choice corresponds to the perturbative branch of the self-energy

$$\Sigma_{\text{bold,perturbative}}(G,V) = \frac{-1 + \sqrt{1+4\,VG^2}}{2G}, \tag{41}$$

and the $-$ to a non-perturbative branch, inaccessible from analytic continuation of the perturbative branch. We stress that the non-invertibility of the mapping $G_0 \to G$ does not have any physical consequence, it does not represent a physical phase transition. However, it has the unfortunate effect of creating an artificial singularity when using the fully-self-consistent diagrammatic formalism at large-enough U.

Misleading convergence. The singularity in the bold self-energy functional can be shown to lead to a misleading convergence of the truncated bold expansion in the zero-dimensional model, where the scheme can converge, albeit slowly, to a wrong solution. More precisely, if we define the Green function sequence G_N

$$G_N^{-1} = G_0^{-1} - \Sigma_{\text{bold},\leq N}(G_N, U), \tag{42}$$

where $\Sigma_{\text{bold},\leq N}(G, V)$ is the N-th order truncated expansion of Σ_{bold} around $V = 0$

$$\Sigma_{\text{bold},\leq N}(G, V) = \sum_{n=1}^{N} V^n \, \Sigma_{\text{bold},n}(G), \tag{43}$$

we find that, due to the presence of this artificial singularity, for large-enough U, G_N converges to the wrong physical answer: $G_N \to \tilde{G} \neq G$, where G is the physical interacting Green function of the Hubbard model corresponding to the non-interacting Green function G_0.
The misleading convergence issue can be avoided by imposing the condition that one is strictly inside the radius of convergence of the shifted action. Indeed, it can be shown that a self-consistent solution of the truncated bold equations does not lead to this misleading convergence issue if this condition is verified.
It has been shown in Ref. [8] that the two-dimensional Hubbard model, at large-enough U, presents this issue. This limits the applicability of the bold formalism in the Hubbard model to weak coupling strengths, where the reliability of the converged result can be verified with this criterion.

4 Computing the expansion: Summing all diagrams to high orders

The main goal of this section is the discussion of the efficient computation of the expansion coefficients $O_{\text{expan},n}$ for a few schemes and quantities. There are three main strategies to evaluate these coefficients: (i) One can enumerate all Feynman diagrams and compute them one-by-one, which is not optimal at high orders and accordingly not discussed in this document; (ii) One can sample different Feynman-diagram topologies, which we rapidly review in Sec. 4.1; (iii) Finally, one can sum over all diagram topologies, symmetrized over the vertex positions, which is justified in Sec. 4.2 and detailed in Sec. 4.3.
More specifically, in Sec. 4.2 we discuss, based both on explicit calculations and general considerations, the computational advantage of summing over all symmetrized diagrams. We also show that summing all Feynman diagrams is an NP-hard problem, which means that we can only expect to solve it in exponential time. Still, exponential algorithms provide a substantial qualitative and quantitative advantage over the enumeration of a factorial number of Feynman diagrams, allowing one to derive the overall polynomial complexity of Sec. 5.1.
Finally, in Sec. 4.3 we show how we can achieve the sum over all symmetrized diagram topologies for various expansions and physical quantities. We end by showing how to perform the remaining integration over the internal vertices thanks to a Markov-chain algorithm over sets.

4.1 Sampling Feynman diagrams

The original form of diagrammatic Monte Carlo consists of sampling diagram topologies. While sampling Feynman diagrams is very flexible as it allows one to directly select the diagram topologies to include in the expansion and is straightforward to formulate in any representation for the edges (notably in the momentum representation), it does not use the strong cancellations between Feynman graphs. For this reason, it generally scales factorially with the expansion order. For a discussion of this sampling algorithm, arguably the "truly diagrammatic" Monte Carlo, see, e.g., Ref. [10–13].

4.2 Why summing all symmetrized Feynman diagrams is important

4.2.1 Spacetime representation and symmetrized sum of all Feynman diagrams

Let O_{phys} be some observable we want to estimate with our diagrammatic Monte Carlo algorithm. We have seen that, in the shifted-action formalism, the observable is obtained by evaluating an expansion function $O_{\text{expan}}(z)$ of an effective coupling constant z for $z{=}1$

$$O_{\text{phys}} = O_{\text{expan}}(z{=}1). \tag{44}$$

The expansion function $O_{\text{expan}}(z)$ is generally known from a power series

$$O_{\text{expan}}(z) = \sum_{n=0}^{N} z^n \, O_{\text{expan},n} + \mathcal{O}(z^{N+1}). \tag{45}$$

It turns out that, in most expansion schemes (we will briefly mention later how to generalize this discussion in other cases), $O_{\text{expan}}(z)$ can be written as a functional of the spacetime-dependent interaction strength, $O_{\text{expan}}[V]$, evaluated for $V(X) = z\,U$

$$O_{\text{expan}}\big[V(X){=}zU\big] = O_{\text{expan}}(z), \tag{46}$$

which means that we can write

$$O_{\text{expan},n} = \frac{1}{n!}\int dX_1 \cdots dX_n \; V(X_1)\cdots V(X_n) \; O_{\text{expan}}(\{X_1,\ldots,X_n\})\Big|_{V(X)=U}, \tag{47}$$

where $O_{\text{expan}}(\{X_1,\ldots,X_n\})$ is the functional derivative with respect to $V(X_1)\cdots V(X_n)$, and it is therefore a function of the *set* of the interaction vertices $X_1,\ldots,X_n$, i.e., it is completely symmetrized with respect to $X_1,\ldots,X_n$.
As an example, we consider the α-shift expansion of Sec. 3.2.3, in which we generalize the chemical-potential shift to a functional of the interaction strength, resulting in a shifted action with quadratic propagator of the form

$$\langle\varphi|G_0^{-1}(z)|\varphi\rangle = \langle\varphi|G_{0;\text{phys}}^{-1}|\varphi\rangle + \,\alpha\,U\langle\varphi|\varphi\rangle - \alpha\int d\mathcal{X}\; V(X)\;(\bar\varphi\varphi)(\mathcal{X})\Big|_{V(X)=z\,U}, \tag{48}$$

which means that $G_0^{-1}(z)$ can be retrieved from a functional of V evaluated at $V(X) = z\,U$, and the same is true for the interaction term, by construction.

The main object of interest in this part of the document is $O_{\text{expan}}(\{X_1, \ldots, X_n\})$, which can be interpreted as the sum of *all* Feynman diagrams in the given expansion scheme with fixed space-time positions of the interaction vertices $X_1, \ldots, X_n$, *symmetrized* over the vertex positions. We justify its importance in the efficient calculation of the expansion in examples below.

4.2.2 Symmetrizing diagrams over vertex positions is important

We consider here an example that shows that the symmetrization over spacetime-vertex positions can be important. We consider the one-site single-species fermionic model

$$\hat{H} = -\mu \hat{N}, \tag{49}$$

where $\hat{N}$ is the particle number, which is either 1 or 0. The partition function is $1{+}e^{\beta\mu}$ and the average particle number is $(1{+}e^{-\beta\mu})^{-1}$. We decide to build the following chemical-potential expansion from half-filling

$$\mu(z) = z. \tag{50}$$

We consider the free energy

$$F(z) = -\frac{1}{\beta} \log Z(z) = -\frac{1}{\beta} \log(1{+}e^{\beta z}) = \sum_{n=0}^{\infty} z^n \, F_n. \tag{51}$$

One notices that $F(z) = -\frac{1}{\beta}\log 2 - z/2 - \frac{1}{\beta}\log\cosh(\beta z/2)$, which implies $F_{2n+1} = 0$ for $n \geq 1$. As the closest singularities of $F(z)$ are at $z{=}{\pm}i\pi/\beta$, we have $F_{2n}{\sim}{-}\frac{1}{\beta}\frac{(-\beta^2)^n}{n\pi^{2n}}$ at large n. We now consider the Feynman-diagram expansion for the free energy in the imaginary-time representation: at order n, there is only one Feynman diagram, with weight proportional to

$$G_0(\tau_1{-}\tau_2)\, G_0(\tau_2{-}\tau_3) \cdots G_0(\tau_n{-}\tau_1), \tag{52}$$

where $\tau_j \in [0, \beta]$ are the imaginary-time positions of the two-point interaction vertices, and $G_0(\tau) = -1/2$ for $\tau \in [0, \beta]$, $G_0(\tau{+}\beta) = -G_0(\tau)$. This shows that

$$\left| G_0(\tau_1{-}\tau_2)\, G_0(\tau_2{-}\tau_3) \cdots G_0(\tau_n{-}\tau_1) \right| = \frac{1}{2^n}\,. \tag{53}$$

This means that cancellations inside this single Feynman diagram when symmetrizing over vertex positions are perfect for odd n, and exponential for even n, as the sum over symmetrized vertex positions is asymptotically $\left(\frac{\pi}{2}\right)^n$ smaller than the absolute value of the weight of the unsymmetrized Feynman diagram (see Fig. 1 for an example at third order).

4.2.3 Summing over all Feynman-diagram topologies is important

We show here that summing over all Feynman-diagram topologies can be important in a specific example. We consider the one-site Hubbard model

$$\hat{H}(z) = -\sum_{\sigma} \mu_\sigma \hat{n}_\sigma + z\, U \hat{n}_\uparrow \hat{n}_\downarrow. \tag{54}$$

Fig. 1: Vertex symmetrization of Feynman diagrams is important. *We show the single Feynman diagram contributing to the chemical potential expansion for the grand potential of the one-site Hubbard model at third order, augmented with all possible (factorial) choices for vertex symmetrization. At half filling, the two contributions shown here cancel exactly.*

The partition function is

$$Z(z) = 1 + \sum_{\sigma} e^{\beta\mu_\sigma} + e^{\beta(\mu_\uparrow+\mu_\downarrow-zU)}. \tag{55}$$

We consider the limit $\beta\mu_\downarrow \to -\infty$, in which the free energy $F(z) = -\frac{1}{\beta}\log Z(z)$ becomes

$$F(z) = -\frac{1}{\beta}\log(1+e^{\beta\mu_\uparrow}) - \frac{1}{\beta}e^{\beta\mu_\downarrow}\frac{1+e^{\beta\mu_\uparrow-\beta zU}}{1+e^{\beta\mu_\uparrow}} + \mathcal{O}(e^{2\beta\mu_\downarrow}), \tag{56}$$

which implies

$$F_n = -\frac{(-\beta U)^n}{\beta\, n!}\frac{e^{\beta\mu_\downarrow}}{1+e^{-\beta\mu_\uparrow}} + \mathcal{O}(e^{2\beta\mu_\downarrow}), \qquad \text{for } n \geq 1. \tag{57}$$

We now consider the Feynman diagrams contributing to the grand potential for a given ordering of the imaginary-time positions of the vertices $\tau_1 < \tau_2 < \cdots < \tau_n$: in the low-density limit for the spin-down particles, the $\downarrow$ lines must connect τ_j with τ_{j+1} to avoid creating subleading negative-time edges, while the up lines can connect vertices without any constraint. This means that the symmetrization over vertex positions does nothing in this limit, and it is therefore an ideal case to study the effect of diagram-topology cancellations. The contribution of a given connected Feynman diagram at fixed imaginary-time positions of the vertices is

$$\Big(\prod_{j=1}^{n} G_{0;\downarrow}(\tau_{j+1}-\tau_j)\Big)\operatorname{sign}\eta \prod_{j=1}^{n} G_{0;\uparrow}(\tau_j-\tau_{\eta_j}), \tag{58}$$

where $\eta \in S_n$ is a permutation of the n vertices and $\tau_{n+1} \equiv \tau_1$. In order to further simplify calculations, we suppose $\mu_\uparrow = 0$, which allows one to write the contribution of a given connected Feynman diagram as

$$\frac{e^{\beta\mu_\downarrow}}{2^n}\operatorname{sign}\eta \prod_{j=1}^{n}\operatorname{sign}(\tau_j-\tau_{\eta_j}), \tag{59}$$

whose absolute value is $e^{\beta\mu_\downarrow}/2^n$ (see Fig. 2 for an example at third order). The time integration contributes $\beta^n/n!$, which needs to be multiplied by the $n!$ Feynman diagrams. Comparing with the exact expression of F_n, $F_n \sim \frac{1}{n!}$, we conclude that there are factorial cancellations between Feynman-diagram topologies. This means that sampling individual Feynman-diagram topologies scales factorially with n in this case.

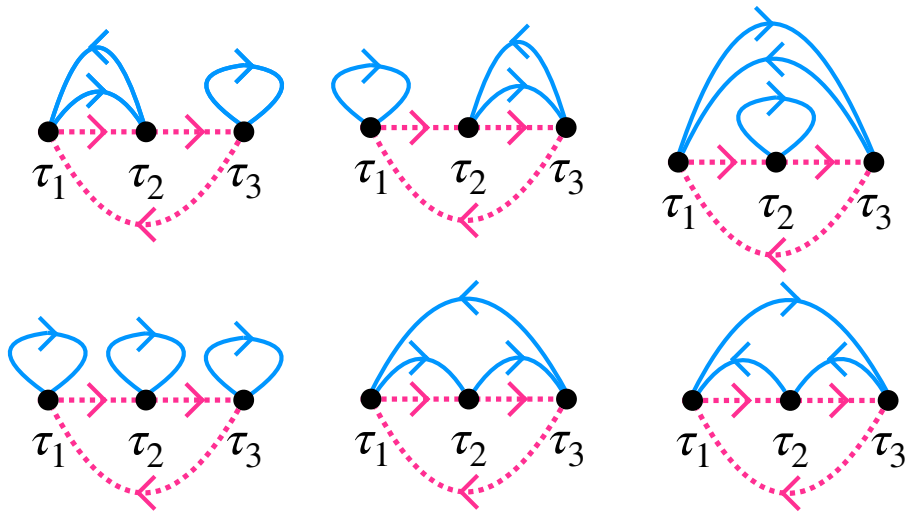

Fig. 2: Summing over all Feynman-diagram topologies is important. *We show all order-three Feynman diagrams contributing to the grand potential of the one-site Hubbard model. We are in the limit where the spin-down chemical potential goes to $-\infty$. We choose $\tau_1 < \tau_2 < \tau_3$, so that vertex symmetrization gives no additional contribution thanks to the low density of spin-down particles. Spin-up propagators are denoted with blue full lines, while spin-down edges are red dashed lines. At half filling, all the factorial Feynman diagrams have the same absolute contribution, but they have different signs, which leads to an almost-perfect cancellation to give an exponential contribution in the order.*

One might additionally argue that the reason for the almost-perfect cancellation really comes from different diagram topologies, and not from the imaginary-time sign of the Green function. Indeed, removing $\mathrm{sign}(\tau_j - \tau_{\eta_j})$ and performing the sum over the Feynman diagrams η gives a zero contribution.

4.3 How to sum all diagrams

We have shown that evaluating the symmetrized sum of all Feynman diagrams is crucial to take advantage of the almost-perfect cancellation of fermionic diagrams. Here we show how to efficiently evaluate the sum of all Feynman diagrams for various quantities and expansions.

4.3.1 Wick's theorem for the sum of all connected and disconnected diagrams

In this section we show that Wick's theorem makes it possible to obtain the sum of all symmetrized Feynman diagrams (see Ref. [14, 15]). We stress that Wick's theorem does not distinguish between connected and disconnected diagrams.
We focus on the calculation of the normalized partition function $\tilde{Z}$ in the bare expansion

$$\tilde{Z}_{\text{bare}}[G_0, z\,V] = \frac{Z_{\text{bare}}[G_0, z\,V]}{Z_{\text{bare}}[G_0, 0]} = \frac{\int D[\varphi,\bar{\varphi}]\; e^{-S_{\text{bare}}[G_0, z\,V]}}{\int D[\varphi,\bar{\varphi}]\; e^{-S_{\text{bare}}[G_0, 0]}} \overset{\star}{=} \sum_{n=0}^{\infty} z^n\, \tilde{Z}_{\text{bare},n}[G_0, V], \qquad (60)$$

where $\overset{\star}{=}$ is used to denote a formal power series, which is just a notation that means that we do not want to discuss here the convergence properties of the series, even if, in this case, the series

is always absolutely convergent. The coefficients of the expansion have the explicit form

$$\tilde{Z}_{\text{bare},n}[G_0, V] = \frac{1}{n!}\int dX_1 \cdots dX_n \; V(X_1)\cdots V(X_n) \; \tilde{Z}_{\text{bare}}[G_0]\big(\{X_1, \ldots, X_n\}\big), \tag{61}$$

where we have introduced the n-th functional derivative with respect to V of the order-n bare-expansion contribution

$$\tilde{Z}_{\text{bare}}[G_0]\big(\{X_1, \ldots, X_n\}\big) := \big\langle (\bar{\varphi}_\uparrow \varphi_\uparrow \bar{\varphi}_\downarrow \varphi_\downarrow)(X_1) \cdots (\bar{\varphi}_\uparrow \varphi_\uparrow \bar{\varphi}_\downarrow \varphi_\downarrow)(X_n) \big\rangle_{S_{\text{bare}}[G_0,0]}. \tag{62}$$

$\tilde{Z}_{\text{bare}}[G_0](\{X_1, \ldots, X_n\})$ is the sum of all Feynman diagrams with fixed spacetime vertex positions $X_1, \ldots, X_n$, symmetrized over permutations of $X_1, \ldots, X_n$. For this reason, we use the set notation $\{X_1, \ldots, X_n\}$ instead of a sequence notation like $(X_1, \ldots, X_n)$.
The action $S_{\text{bare}}[G_0, 0]$ is quadratic in φ and $\bar{\varphi}$: this means that we can compute moments exactly with Wick's theorem: any Gaussian average of monomials of the Grassmann fields is equal to the sum over all possible products of contractions of $G_0(\mathcal{X}, \mathcal{Y}) = -\langle \varphi(\mathcal{X})\bar{\varphi}(\mathcal{Y})\rangle$, with a proper sign coming from fermionic exchange

$$(-1)^m \big\langle \varphi(\mathcal{X}_1)\bar{\varphi}(\mathcal{Y}_1)\cdots\varphi(\mathcal{X}_m)\bar{\varphi}(\mathcal{Y}_m)\big\rangle_{S_{\text{bare}}[G_0,0]} = \sum_{\sigma\in S_m} \text{sign}\;\sigma \prod_{j=1}^{m} G_0(\mathcal{X}_j, \mathcal{Y}_{\sigma_j}) = \det \mathbb{G}_0, \tag{63}$$

where the $m\times m$ matrix $\mathbb{G}_0$ is defined by

$$[\mathbb{G}_0]_{jk} = G_0(\mathcal{X}_j, \mathcal{Y}_k). \tag{64}$$

This determinantal form of Wick's theorem, which is well known and used in various quantum Monte Carlo algorithms, shows that we can compute the symmetrized sum of a factorial number of Feynman diagrams with an effort that only increases polynomially with the order of the expansion. For the particular case of the Hubbard model, we can compute the $n!$ diagrams symmetrized over $n!$ permutations of the vertices, which define $\tilde{Z}_{\text{bare}}[G_0](\{X_1, \ldots, X_n\})$, in $\mathcal{O}(n^3)$ time, which is a remarkable result given the large number of symmetrized Feynman diagrams. However, the diagrams we can compute with Wick's theorem are partition function diagrams, and not all of them are well-defined in the thermodynamic limit. In order to obtain diagrammatic expansions for physical observables such as the free energy density, which has a well-defined thermodynamic limit, we need to remove disconnected diagrams from the partition function, as shown in the rest of this section.

4.3.2 Computing the contribution of connected Feynman diagrams is NP-hard

We have seen in the specific case of the bare expansion of the Hubbard model that we can evaluate the sum of all diagrams, connected and disconnected, in a time increasing polynomially with the order of the expansion. One might expect that the task of removing disconnected diagrams from this sum is rather easy, and maybe hope for a polynomial-time algorithm. Instead, we show here that evaluating the contribution of order-n connected Feynman diagrams is NP-hard.

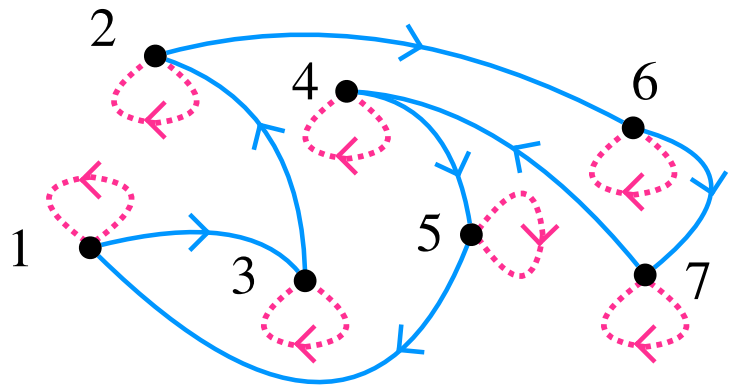

Fig. 3: Computing the contribution of connected Feynman diagrams is NP-hard. *If a general algorithm to compute the symmetrized sum of all connected Feynman diagrams in polynomial time for the Hubbard model existed, then it could be used to solve all NP problems in polynomial time. Shown here is a connected Feynman diagram of a Hubbard-like model with a diverging chemical potential for the spin-down particle. The sum of all such connected Feynman diagrams gives the Hamiltonian cycle polynomial of the graph with the $\mathbb{G}_{0;\uparrow}$ matrix.*

More precisely, we are going to show that evaluating the n-th coefficient of the bare expansion, built from connected Feynman diagrams, for a general G_0, is NP-hard. For this proof, it is sufficient to consider a discretized spacetime with indices j, and the Grassmann action

$$S_{\text{bare}}[G_0](z) = -\sum_{\sigma\in\{\uparrow,\downarrow\};j,k=1}^{n} \bar{\varphi}_{\sigma;j}\left[G_0^{-1}\right]_{\sigma;jk}\varphi_{\sigma;k} + z\sum_{j=1}^{n}\bar{\varphi}_{\uparrow;j}\varphi_{\uparrow;j}\bar{\varphi}_{\downarrow;j}\varphi_{\downarrow;j}. \tag{65}$$

For this proof, we consider

$$G_{0;\downarrow,jk} = \delta_{jk}, \tag{66}$$

while $G_{0;\uparrow,jk}$ is arbitrary. This choice makes the interaction effectively one-body. Accordingly, there is only one Feynman diagram contributing at order n, which is built from $G_{0;\uparrow}$ lines and trivial tadpole lines for $G_{0;\downarrow}$ (see Fig. 3). This means that the total order-n integrated contribution is, by construction, given by the symmetrization of this single Feynman diagram

$$\left(\prod_{j=1}^{n} G_{0;\downarrow;jj}\right)\sum_{\eta\in H_n}\prod_{j=1}^{n} G_{0;\uparrow;j\eta_j}, \tag{67}$$

where H_n is the set of permutations of the vertices $1,\ldots,n$ having exactly one cycle. The term $\sum_{\eta\in H_n}\prod_{j=1}^{n} G_{0;\uparrow;j\eta_j}$ is the Hamiltonian cycle polynomial with connectivity matrix $G_{0;\uparrow;jk}$. This means that the existence of a Hamiltonian cycle of a general graph, which is an NP-complete problem (see Ref. [16–18]), could be detected by the evaluation of this polynomial for a special choice of the matrix $G_{0;\uparrow;jk}$. This means that computing the order n contribution, either by sampling Feynman diagrams or with any other algorithm to compute the sum, is a hard, almost-surely exponential, problem.

In practice, this means that we should not expect the existence of generic polynomial-time algorithms to evaluate connected symmetrized Feynman-diagram contributions. For instance,

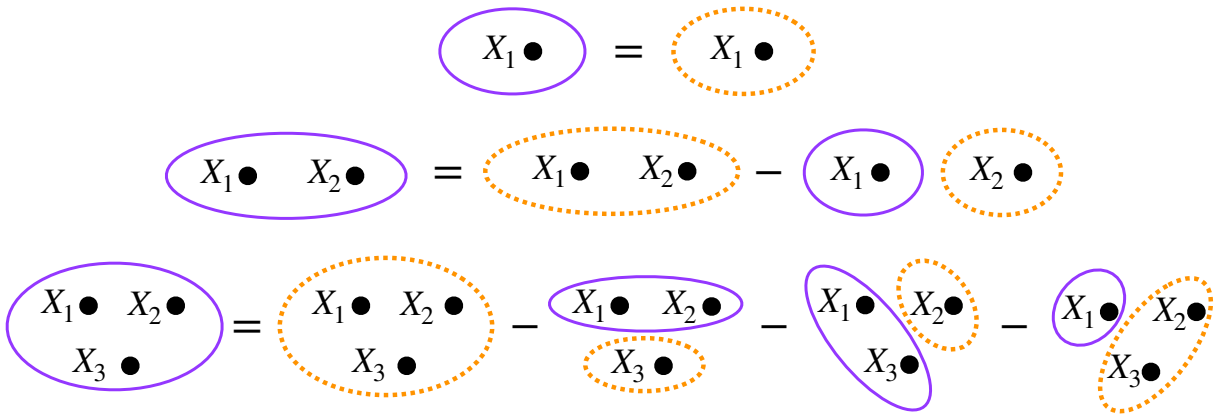

Fig. 4: Recursive formula to remove disconnected Feynman diagrams. *Dashed-line orange sets represent $\tilde{Z}(S)$, the sum of all Feynman diagrams (connected+disconnected) contributing to the partition function, while full-line violet sets correspond to $\tilde{\Omega}(S)$. Shown is the recursive formula to obtain $\tilde{\Omega}(S)$ from the knowledge of $\tilde{Z}(S')$ for $S' \subseteq S$.*

the Held-Karp algorithm can be adapted to compute the Hamiltonian cycle polynomial relevant to the one-body expansion we have discussed in the proof. It has a run-time of $\mathcal{O}(n^2\,2^n)$ for an n-th vertex graph. For a k-body interaction, with $k > 1$, we certainly should not expect a meaningfully faster runtime.

4.3.3 The connected determinant approach

Diagrams contributing to physical observables with a proper thermodynamic limit must be connected. We have shown that computing connected Feynman diagrams is NP-hard, so we should not expect a faster-than-exponential algorithm to compute them. The purpose of this section is to show a general k-body algorithm to compute symmetrized connected Feynman diagrams contributing to the bare expansion. The runtime of this so-called "connected-determinant" method (see Ref. [19]) scales as $\mathcal{O}(3^n)$, which can be asymptotically improved to $\mathcal{O}(n^2\,2^n)$ using fast subset convolution techniques (introduced in Ref. [20]), even if not practical for the typical n values encountered.

We write the bare-expansion grand potential

$$\Omega_{\text{bare}}[G_0, z\,V] = -\frac{1}{\beta}\log Z_{\text{bare}}[G_0, z\,V] = \Omega_{\text{bare}}[G_0, 0] - \frac{1}{\beta}\log \tilde{Z}_{\text{bare}}[G_0, z\,V]. \tag{68}$$

To simplify the formulas, it is useful to introduce

$$\tilde{\Omega}_{\text{bare}}[G_0, V] := \log \tilde{Z}_{\text{bare}}[G_0, V], \tag{69}$$

which we expand in formal power series in z

$$\tilde{\Omega}_{\text{bare}}[G_0, z\,V] \stackrel{\star}{=} \sum_{n=0}^{\infty} z^n\, \tilde{\Omega}_{\text{bare},n}[G_0, V], \tag{70}$$

where

$$\tilde{\Omega}_{\text{bare},n}[G_0, V] = \frac{1}{n!}\int dX_1 \cdots dX_n\, V(X_1)\cdots V(X_n)\, \tilde{\Omega}_{\text{bare}}[G_0]\big(\{X_1, \ldots, X_n\}\big). \tag{71}$$

$\tilde{\Omega}_{\text{bare}}[G_0](\{X_1,\ldots,X_n\})$ is the sum of all connected Feynman diagrams with fixed spacetime vertex positions $X_1,\ldots,X_n$, symmetrized with respect to the vertex positions. We simplify here the notation by dropping "bare" and the explicit G_0 dependence:

$$\begin{aligned}\tilde{\Omega}_{\text{bare}}[G_0](\{X_1,\ldots,X_n\}) &\mapsto \tilde{\Omega}(\{X_1,\ldots,X_n\}),\\ \tilde{Z}_{\text{bare}}[G_0](\{X_1,\ldots,X_n\}) &\mapsto \tilde{Z}(\{X_1,\ldots,X_n\}).\end{aligned} \tag{72}$$

By expanding the logarithm, we can express $\tilde{\Omega}$ in terms of the easy-to-compute $\tilde{Z}(S)$. Explicitly

$$\tilde{\Omega}(\{X_1\}) = \tilde{Z}(\{X_1\}), \tag{73}$$

$$\tilde{\Omega}(\{X_1,X_2\}) = \tilde{Z}(\{X_1,X_2\}) - \tilde{Z}(\{X_1\})\,\tilde{Z}(\{X_2\}), \tag{74}$$

$$\begin{aligned}\tilde{\Omega}(\{X_1,X_2,X_3\}) = \tilde{Z}(\{X_1,X_2,X_3\}) &- \tilde{Z}(\{X_1\})\,\tilde{Z}(\{X_2,X_3\}) - \tilde{Z}(\{X_2\})\,\tilde{Z}(\{X_1,X_3\})\\ &- \tilde{Z}(\{X_3\})\,\tilde{Z}(\{X_1,X_2\}) + 2\,\tilde{Z}(\{X_1\})\,\tilde{Z}(\{X_2\})\,\tilde{Z}(\{X_3\}),\end{aligned} \tag{75}$$

and so on. These expressions for computing $\tilde{\Omega}(S)$ given $\tilde{Z}(S')$ for all $S' \subseteq S$ are not very efficient as the number of terms is equal to the number of possible partitions of a set of n elements, the Bell number, which grows factorially with n.
Using the fact that $\tilde{\Omega}(S)$ represents the sum of all connected Feynman diagrams with spacetime vertex positions at S, we can derive the more efficient recursive formula

$$\tilde{\Omega}(S) = \tilde{Z}(S) - \sum_{S'\subsetneq S\backslash\{X_1\}} \tilde{\Omega}\big(\{X_1\}\cup S'\big)\,\tilde{Z}\big(S\backslash S'\backslash\{X_1\}\big), \tag{76}$$

which has the interpretation of removing from $\tilde{Z}(S)$ the diagrams that can be split in a part connected to the vertex $\{X_1\}$, represented by $\tilde{\Omega}\big(\{X_1\}\cup S'\big)$, and another part of the diagram that is disconnected from it, $\tilde{Z}\big(S\backslash S'\backslash\{X_1\}\big)$. See Fig. 4 for a graphical interpretation of the recursive formula.
The number of arithmetic operations needed to obtain $\tilde{\Omega}(S)$ from $\tilde{Z}$ is $\mathcal{O}(3^n)$, as we now show. Let $\tilde{\Omega}_{X_1}(S) = \tilde{\Omega}(\{X_1\}\cup S)$. Assuming $\tilde{\Omega}_{X_1}(S')$ and $\tilde{Z}(S')$ are known for all $S'\subsetneq S$: one can apply the recursive formula to obtain $\tilde{\Omega}_{X_1}(S)$ with a number of multiplications equal to $2^{|S|}-1$ and a number of additions equal to $2^{|S|}$. Ignoring the additions, the total number of multiplications to obtain $\tilde{\Omega}_{X_1}(S)$ is

$$\sum_{S'\subsetneq S}\Big(2^{|S'|}-1\Big) = \sum_{k=0}^{|S|}\binom{|S|}{k}2^k - 2^{|S|+1} + 1 = 3^{n-1} - 2^n + 1, \tag{77}$$

where we have used the fact that $|S| = n-1$.

4.3.4 Algebraic formulation: nilpotent polynomials

In order to allow for generalization of the formalism we have developed, it is convenient to introduce so-called nilpotent polynomials.

Nilpotent polynomials are an automatic tool to compute functional derivatives of functionals. They are based on nilpotent symbols η_j with the following properties

$$\eta_j^2 = 0, \qquad \eta_j \eta_k = \eta_k \eta_j, \tag{78}$$

where $j, k \in \{1, \dots, n\}$. Let $F[V]$ be a functional of the variable $V(X)$

$$F[V] \stackrel{\star}{=} \sum_{k=0}^{\infty} \frac{1}{k!} \int dX_1 \cdots dX_k \; V(X_1) \cdots V(X_k) \; F\big(\{X_1, \dots, X_k\}\big). \tag{79}$$

If the functional is evaluated for $V_\eta(X) = \sum_{j=1}^{n} \delta(X - X_j) \, \eta_j$, we have

$$F[V{=}V_\eta] = \sum_{S \subseteq \{X_1, \cdots, X_n\}} F(S) \, \eta(S), \tag{80}$$

where we have introduced $\eta(S) := \prod_{X_j \in S} \eta_j$. This means that, if our goal is to compute high-order functional derivatives with respect to the field $V(X)$, we can look at the coefficients of the functional when evaluated with V_η. While this does not sound very useful when only one functional $F[V]$ is involved, it becomes extremely convenient when considering combinations of functionals. For example, assume that we know the functional derivatives of two functionals $F_1[V]$ and $F_2[V]$, and suppose we want to compute the functional derivatives of their product

$$F_3[V] = F_1[V] \; F_2[V]. \tag{81}$$

For this, we can evaluate $F_j[V]$ for $V = V_\eta$

$$F_j[V] = \sum_{S \subseteq \{X_1, \dots, X_n\}} F_j(S) \; \eta(S), \tag{82}$$

which allows one to write

$$\sum_{S_3 \subseteq \{X_1, \dots, X_n\}} F_3(S_3) \; \eta(S_3) = \sum_{S_1, S_2 \subseteq \{X_1, \dots, X_n\}} F_1(S_1) \; F_2(S_2) \; \eta(S_1) \; \eta(S_2). \tag{83}$$

Using

$$\eta(S_1) \; \eta(S_2) = \begin{cases} \eta(S_1 \cup S_2) & \text{if } \; S_1 \cap S_2 = \emptyset \\ 0 & \text{otherwise} \end{cases}, \tag{84}$$

we obtain

$$F_3(S_3) = \sum_{S_1 \subseteq S_3} F_1(S_1) \; F_2(S_3 \backslash S_1), \tag{85}$$

which allows one to express the functional derivatives of F_3 in terms of functional derivatives of F_1 and F_2. We can also interpret the previous formulation in terms of operations between nilpotent polynomials, i.e., polynomials in the nilpotent variables $\eta_1, \dots, \eta_n$, which we denote by $F_j[[\boldsymbol{\eta}]]$

$$F_3[[\boldsymbol{\eta}]] = F_1[[\boldsymbol{\eta}]] \; F_2[[\boldsymbol{\eta}]]. \tag{86}$$

We have already mentioned that the sum of all Feynman diagrams symmetrized over the fixed positions of spacetime vertices corresponds to a functional derivative of the expansion functional with respect to the interaction (see Eq. (47)). This means that we can use nilpotent polynomials to efficiently manipulate such functional derivatives. Moreover, they can be useful for generalizing the formalism to shifted-action renormalization.

Let us reproduce the connected-determinant derivation from this purely-algebraic nilpotent-polynomial formulation. We evaluate the functionals $\tilde{\Omega}_{\text{bare}}[G_0, V]$ and $\tilde{Z}_{\text{bare}}[G_0, V]$ for $V = V_\eta$

$$\sum_{S\subseteq\{X_1,\ldots,X_n\}} \tilde{\Omega}(S)\ \eta(S) = \log\Big(\sum_{S\subseteq\{X_1,\ldots,X_n\}} \tilde{Z}(S)\ \eta(S)\Big). \tag{87}$$

Equivalently, in terms of nilpotent polynomials

$$\tilde{\Omega}[[\boldsymbol{\eta}]] = \log \tilde{Z}[[\boldsymbol{\eta}]], \tag{88}$$

which means that computing all grand-potential connected diagrams is equivalent to taking the logarithm of a nilpotent polynomial.

In order to efficiently evaluate the logarithm, we take the derivative of both sides with respect to η_1, and we set η_1 to zero afterwards (this is to avoid null terms like $\eta_1^2 = 0$ having a non-zero contribution $2\,\eta_1 \neq 0$ to the derivative)

$$\sum_{S\subseteq\{X_2,\ldots,X_n\}} \tilde{\Omega}\big(\{X_1\}\cup S\big)\ \eta(S) = \frac{\sum_{S\subseteq\{X_2,\ldots,X_n\}} \tilde{Z}\big(\{X_1\}\cup S\big)\ \eta(S)}{\sum_{S\subseteq\{X_2,\ldots,X_n\}} \tilde{Z}(S)\ \eta(S)}, \tag{89}$$

which we rewrite as

$$\sum_{S',S''\subseteq\{X_2,\ldots,X_n\}} \tilde{\Omega}\big(\{X_1\}\cup S'\big)\ \tilde{Z}(S'')\ \eta(S')\ \eta(S'') = \sum_{S\subseteq\{X_2,\ldots,X_n\}} Z\big(\{X_1\}\cup S\big)\ \eta(S). \tag{90}$$

Using Eq. (84), we immediately recognize the previous equation as equivalent to Eq. (76).

4.3.5 Bare-expansion functional for the Green function

The connected determinant formalism can be applied to correlation functions as well. Here we use the nilpotent-polynomial algebraic formulation. We illustrate the method for the case of the bare expansion for the one-particle Green function

$$G_{\text{bare};\mathcal{Y},\mathcal{Y}'}[G_0, zV] = -\frac{\int\mathcal{D}[\varphi,\bar{\varphi}]\ e^{-S_{\text{bare}}[G_0,zV]}\ \varphi(\mathcal{Y})\ \bar{\varphi}(\mathcal{Y}')}{\int\mathcal{D}[\varphi,\bar{\varphi}]\ e^{-S_{\text{bare}}[G_0,zV]}} = \frac{A_{\text{bare};\mathcal{Y},\mathcal{Y}'}[G_0, zV]}{\tilde{Z}_{\text{bare}}[G_0, zV]}\,. \tag{91}$$

In analogy to what was done before for $\tilde{Z}$, we expand A in a formal series in z

$$A_{\text{bare};\mathcal{Y},\mathcal{Y}'}[G_0, z\,V] \stackrel{\star}{=} \sum_{n=0}^{\infty} \frac{z^n}{n!}\int dX_1\cdots dX_n\ V(X_1)\cdots V(X_n)\ A_{\text{bare};\mathcal{Y},\mathcal{Y}'}[G_0](\{X_1,\ldots,X_n\}). \tag{92}$$

Using Wick's theorem, Eq. (63), it is possible to compute $A_{\text{bare};\mathcal{Y},\mathcal{Y}'}[G_0](S)$ and $\tilde{Z}_{\text{bare}}[G_0](S)$ in polynomial-in-n time for any set of vertex positions S in terms of determinants involving

matrices built from the non-interacting Green function G_0. In terms of Feynman diagrams, $A_{\text{bare};\mathcal{Y},\mathcal{Y}'}(S)$ is the sum of all (i.e. connected and disconnected) symmetrized diagrams with S as internal vertices and having $\mathcal{Y}$ and $\mathcal{Y}'$ as external vertices.
Using the nilpotent polynomial formalism, it is immediate to derive $G_{\text{bare};\mathcal{Y},\mathcal{Y}'}[G_0](S)$: as before, we evaluate the functional $G_{\text{bare};\mathcal{Y},\mathcal{Y}'}[G_0, V]$ for $V(X) = V_\eta(X) = \sum_{j=1}^{n} \delta(X - X_j)\, \eta_j$

$$G_{\text{bare};\mathcal{Y},\mathcal{Y}'}[G_0, V_\eta] = \frac{A_{\text{bare};\mathcal{Y},\mathcal{Y}'}[G_0, V_\eta]}{\tilde{Z}_{\text{bare}}[G_0, V_\eta]}, \tag{93}$$

which is equivalent, by definition, to

$$G_{\text{bare};\mathcal{Y},\mathcal{Y}'}[[\boldsymbol{\eta}]] = \frac{A_{\text{bare};\mathcal{Y},\mathcal{Y}'}[[\boldsymbol{\eta}]]}{\tilde{Z}_{\text{bare}}[[\boldsymbol{\eta}]]}, \tag{94}$$

which means that computing connected diagrams for the Green function is equivalent to a nilpotent polynomial division.
In order to efficiently evaluate the nilpotent polynomial division, we write

$$G_{\text{bare};\mathcal{Y},\mathcal{Y}'}[[\boldsymbol{\eta}]]\ \tilde{Z}_{\text{bare}}[[\boldsymbol{\eta}]] = A_{\text{bare};\mathcal{Y},\mathcal{Y}'}[[\boldsymbol{\eta}]]. \tag{95}$$

The latter equation is a multiplication between nilpotent polynomials, which we know how to perform. Specifically, after removing the "bare" label and the explicit G_0 dependence

$$\sum_{S' \subseteq \{X_1,\dots,X_n\}} G_{\mathcal{Y},\mathcal{Y}'}(S') \sum_{S'' \subseteq \{X_1,\dots,X_n\}} \tilde{Z}(S'')\ \eta(S')\, \eta(S'') = \sum_{S \subseteq \{X_1,\dots,X_n\}} A_{\mathcal{Y},\mathcal{Y}'}(S)\ \eta(S), \tag{96}$$

which means that we can obtain a recursive relation for the Green function bare-expansion functional

$$G_{\mathcal{Y},\mathcal{Y}'}(S) = A_{\mathcal{Y},\mathcal{Y}'}(S) - \sum_{S' \subsetneq S} G_{\mathcal{Y},\mathcal{Y}'}(S')\ \tilde{Z}(S \backslash S'), \tag{97}$$

for all $S \subseteq \{X_1, \dots, X_n\}$, where we have used $\tilde{Z}(\emptyset) = 1$.

4.3.6 Self-energy

In order to compute one-particle properties, it is often advantageous to compute the self-energy instead of the Green function. In this section we describe the algorithm to build the bare-expansion self-energy functional used, e.g., in Ref. [21].
We specialize here the discussion to the bare spin-balanced normal-phase expansion for a translation-invariant system

$$G_0(\mathcal{Y}, \mathcal{Y}') = \delta_{\sigma,\sigma'}\ G_{0;\sigma}(Y - Y'), \tag{98}$$

where $\mathcal{Y} = (\sigma, Y)$, $\mathcal{Y}' = (\sigma', Y')$. In this case, Wick's theorem implies

$$\tilde{Z}_{\text{bare}}[G_0](S) = (-1)^{|S|}\ \det\, \mathbb{G}_{0;\uparrow}(S)\, \det \mathbb{G}_{0;\downarrow}(S), \tag{99}$$

where $S = \{X_1, \ldots, X_{|S|}\}$, and where we have introduced the matrix $[\mathbb{G}_{0;\sigma}(S)]^{jk} = G_{0;\sigma}(X_j, X_k)$ for $X_j, X_k \in S$.

We define the auxiliary quantity $\mathcal{A}$

$$\mathcal{A}_{\text{bare};\sigma;jk}[G_0](S) = \frac{\partial}{\partial G_{0;\sigma}(X_k, X_j)} \tilde{Z}_{\text{bare}}[G_0](S) = (-1)^{|S|} \, [\text{adj}\, \mathbb{G}_{0;\sigma}(S)]_{jk} \; \det \, \mathbb{G}_{0;-\sigma}(S), \tag{100}$$

where adj means the adjugate of a matrix. The diagrammatic interpretation of the function $\mathcal{A}_{\text{bare};\sigma,X_j,X_k}[G_0](S)$ is the sum of all diagrams for the partition function with fixed spacetime vertices S in which we remove a $G_{0;\sigma}(X_k, X_j)$ line.

From now on we impose, for simplicity, $G_{0;\uparrow} = G_{0;\downarrow}$. In order to remove disconnected diagrams, we can remove all diagrams that factorize in a partition function diagram and the connected part

$$\Xi_{jk}(S) = \mathcal{A}_{jk}(S) - \sum_{S' \subsetneq S} \Xi_{jk}(S') \; \tilde{Z}(S \backslash S'), \tag{101}$$

where we have identified vertices like X_k with their index k, and where we have used a shorthand notation for $\mathcal{A}_{\text{bare}}$, $\tilde{Z}_{\text{bare}}$ and Ξ_{bare}, the latter being an auxiliary quantity equal to the sum of all connected Feynman diagrams contributing to $\mathcal{A}_{\text{bare}}$, which is zero for $S = \emptyset$.

We introduce another auxiliary quantity ρ, defined by

$$\rho^j_k(S) = \sum_{l:\, X_l \in S} G_0(X_j, X_l) \; \Xi_{lk}(S), \tag{102}$$

for $X_j \notin S$.

We now have all the ingredients to evaluate the bare self-energy. The Hartree contribution Σ_{jj} is simply

$$\Sigma_{jj}(S) = \Xi_{jj}(S), \tag{103}$$

where $X_j \in S$. The non-Hartree contribution can be obtained from

$$\Sigma_{jk}(S) = \Xi_{jk}(S) - \sum_{l, S' \subsetneq S} \Sigma_{jl}(S') \; \rho^l_k(S \backslash S'), \tag{104}$$

where $X_j, X_k \in S$, $X_j \neq X_k$. Diagrammatically, Eq. (104) means that we are removing from Ξ all diagrams that can be split in a one-particle-irreducible part, $\Sigma_{jl}(S')$, and the convolution of a G_0 line with another piece, $\rho^l_k(S \backslash S')$. Algebraically, we are writing the self-energy as

$$\Sigma \, G \, G_0^{-1} = G_0^{-1} \, G \, G_0^{-1} - G_0^{-1}, \tag{105}$$

where $\rho = G \, G_0^{-1}$ and $\Xi = G_0^{-1} \, G \, G_0^{-1} - G_0^{-1}$. In order to derive Eq. (104) and Eq. (103), we could have then used

$$\boldsymbol{\Sigma}[[\boldsymbol{\eta}]] \; \boldsymbol{\rho}[[\boldsymbol{\eta}]] = \boldsymbol{\Xi}[[\boldsymbol{\eta}]], \tag{106}$$

where $\boldsymbol{\Sigma}[[\boldsymbol{\eta}]]$, $\boldsymbol{\rho}[[\boldsymbol{\eta}]]$ and $\boldsymbol{\Xi}[[\boldsymbol{\eta}]]$ are nilpotent-polynomial-valued matrices, and where we have defined $\boldsymbol{\rho}(\emptyset) = \mathbb{I}$.

For a translation-invariant system, it is convenient to measure the self-energy directly in momentum space. This can be achieved by defining the Fourier transform of the non-Hartree part of the self-energy for a given set of interaction vertices S

$$\Sigma_K^{NH}(S) = \frac{1}{|S|(|S|-1)} \sum_{j \neq k} \Sigma_{jk}(S)\ e^{-iK\cdot(X_j - X_k)}, \tag{107}$$

where $K = (i\omega_n, \boldsymbol{k})$ is a collective momentum variable made of a fermionic Matsubara frequency ω_n and a spatial momentum $\boldsymbol{k}$. The Hartree part of the self-energy gives a constant contribution to the momentum self-energy.
In terms of computational cost, to compute the sum of all one-particle-irreducible diagrams with n vertices, symmetrized over the vertex positions and over the n^2 possible choices of pairs for the external points, the algorithm requires computing 2^n determinants and adjugates, which can be done in $\mathcal{O}(n^3\, 2^n)$ or faster, and $\mathcal{O}(n^2\, 3^n)$ for the elimination of disconnected and one-particle reducible diagrams.

4.3.7 One-particle renormalization

We have seen that within the shifted-action formalism, one-particle renormalization can be achieved by letting the non-interacting one-particle propagator be a function of the coupling constant z

$$S_{\text{bare}}[G_0(z), z\, V]. \tag{108}$$

Diagrammatically, it is natural to consider expansion schemes such that subdiagrams consisting of low-order self-energy insertions do not contribute at higher orders. This procedure can be applied at various levels of self-consistency, either at the functional level or at the z-function level, the latter being beyond the scope of this document.
We decide here to focus on the most challenging-to-derive algorithm for one-particle renormalization: the full renormalization of the one-particle propagator. Most of the other possible expansion schemes are specializations or adaptations of this algorithm in simpler settings, which justifies the choice of including the bold expansion in this document. The bold expansion scheme is defined by (see also Eq. (37) and Eq. (38))

$$G_{0;\text{bold}}[G, V]^{-1} = G^{-1} + \Sigma_{\text{bold}}[G, V]. \tag{109}$$

We fix the order of the expansion to n, and then fix a given set of n vertices, $E = \{X_1, \ldots, X_n\}$. We write Eq. (109) as a nilpotent polynomial equation by evaluating the functionals for $V = V_\eta$, and we drop the G dependence

$$\mathbb{G}_{0;\text{bold}}[[\boldsymbol{\eta}]] = \mathbb{G} - \mathbb{G}_{0;\text{bold}}[[\boldsymbol{\eta}]]\ \boldsymbol{\Sigma}_{\text{bold}}[[\boldsymbol{\eta}]]\ \mathbb{G}, \tag{110}$$

where $\mathbb{G}_{0;\text{bold}}$, $\boldsymbol{\Sigma}$ and $\mathbb{G}$ are $n \times n$ matrices. The difficulty of solving the previous equation for $\mathbb{G}_{0;\text{bold}}[[\boldsymbol{\eta}]]$ is that $\boldsymbol{\Sigma}_{\text{bold}}[[\boldsymbol{\eta}]]$ is an unknown functional of G to be determined from the equation

$$\boldsymbol{\Sigma}_{\text{bare}}[\mathbb{G}_{0;\text{bold}}[[\boldsymbol{\eta}]]][[\boldsymbol{\eta}]] = \boldsymbol{\Sigma}_{\text{bold}}[[\boldsymbol{\eta}]]. \tag{111}$$

Suppose that we have determined $\boldsymbol{\Sigma}_{\text{bold}}(S)$ for all $S \subseteq E$ with $|S| \leq k$. We can then first obtain $\boldsymbol{\Sigma}_{\text{bold}}(S)\,\mathbb{G}$, and then compute $\mathbb{G}_{0;\text{bold}}(S)$ for $|S| \leq k$ from Eq. (110). The crucial observation is that, in order to obtain $\boldsymbol{\Sigma}_{\text{bold}}(S')$ for $|S'| = k{+}1$ we only need to know $\mathbb{G}_{0;\text{bold}}(S)$ for $|S| \leq k$, which means that we can solve Eq. (111) recursively. More specifically, in order to build the nilpotent polynomial $\boldsymbol{\Sigma}_{\text{bare}}[\mathbb{G}_{0;\text{bold}}[[\boldsymbol{\eta}]]][[\boldsymbol{\eta}]]$ for $|S| = k{+}1$ we need to compute $\boldsymbol{\mathcal{A}}$ by using $G_{0;\text{bold}}[[\boldsymbol{\eta}]]$, computing $\boldsymbol{\Xi}$, $\boldsymbol{\rho}$, and finally $\boldsymbol{\Sigma}_{\text{bare}}$. Formally, the algorithm is identical to the bare one, the only difference being that the operations must be done in the ring of nilpotent polynomials.

In terms of computational cost, the computation of $\mathcal{A}$ is the most expensive part. $\mathcal{A}(S)$ involves computing the adjugate and the determinant of a matrix containing nilpotent polynomials in $|S|$ variables, whose cost can be bounded assuming the use of the naive Gaussian elimination by $\mathcal{O}(|S|^3\,3^{|S|})$. This means that the total cost to compute the sum of all symmetrized skeleton diagrams contributing to the self-energy for all pairs of vertices as external points is bounded by $\mathcal{O}(n^3\,4^n)$, much better than the $\mathcal{O}(n^2\,(n!)^2)$ naive enumeration cost. This derivation is useful as a similar methodology can be used for many other one-particle renormalization schemes. Ref. [22] presents a method based on the combinatorial summation of Feynman diagrams that is able to reduce the scaling of the evaluation of bold functionals to $\mathcal{O}(n^3\,3^n)$.

4.3.8 Sampling vertex positions with Many-Configuration Markov-Chain Monte Carlo

Integrating over vertex positions. So far we have discussed how to compute the sum of all symmetrized Feynman diagrams for a given quantity O in a given expansion scheme at fixed spacetime positions $X_1, \ldots, X_n$ of the interaction vertices, which we call $O_{\text{expan}}(\{X_1, \ldots, X_n\})$. The purpose of this section is to show how to perform the integration over the positions of the internal ensemble of vertices $\{X_1, \ldots, X_n\}$

$$O_{\text{expan},n} = \frac{1}{n!}\int dX_1 \cdots dX_n\; V(X_1)\cdots V(X_n)\; O_{\text{expan}}\big(\{X_1, \ldots, X_n\}\big), \tag{112}$$

to obtain the final estimate for the order-n coefficient of the expansion, $O_{\text{expan},n}$. The integration over $X_1, \ldots, X_n$ does not present many difficulties. Even for an infinite system, as we are computing connected quantities, $X_1, \ldots, X_n$ cluster together and the integral is finite (a trivial exception being the grand potential, where one has to fix the position of one of the vertices to compute the well-defined grand-potential density).

For the d-dimensional Hubbard model, the integration runs over d spatial components and one imaginary time component, making the total number of integration variables equal to $(d{+}1)n$ for an order n calculation. As $n = \mathcal{O}(10)$, the integration is high-dimensional and not amenable to most deterministic techniques. For this reason, the use of Monte Carlo sampling is essential to obtain a statistical estimate of the value of the integral. A simple order-changing Markov-chain Monte Carlo algorithm that includes an order-changing update is sufficient to obtain an estimate of the integral. However, as a byproduct of the diagram summing procedure we have calculated $O_{\text{expan}}(S)$ for all $S \subseteq \{X_1, \ldots, X_n\}$, and therefore it is natural to look for more efficient ways to use that information. Essentially, at fixed n, we would like to consider all configurations S

as possible updates for the Markov-chain Monte Carlo procedure. This is achieved with the Many-configuration Markov-chain Monte Carlo algorithm (MC^3) (see Ref. [23]), which we briefly sketch below.

Markov-chain of sets of configurations. In the following, we use for simplicity of presentation a lighter notation. Suppose the goal is to obtain a Monte Carlo estimate of integrals of this form

$$O_k = \sum_{S\subseteq\mathcal{E}:\ |S|=k} O(S), \tag{113}$$

for $k \in \{0, 1, \ldots, n\}$, where $\mathcal{E}$ is an abstract set (aka ensemble) defining the configuration space. Suppose that, given an ensemble E contained in $\mathcal{E}$, $E \subseteq \mathcal{E}$, one has automatically obtained in some way all $O(S)$ for each subset S of E, $S \subseteq E$. The challenge is to find an efficient Markov-chain Monte Carlo algorithm that maximally takes advantage of this information. One could consider taking an equilibrium probability distribution for the Markov chain proportional to $|O(S)|$, and perform a Markov chain over sets of different cardinality. The problem is that, with this formulation, only the information on one set S is used at each Monte Carlo step. We are therefore led to consider some sort of all-subset probability distribution of the form $\sum_{S\subseteq E}\ |O(S)|$. The problem with the latter attempt is that we are summing over functions with a different number of variables, and therefore we cannot even define the configuration space for the Markov chain. This can be solved in the following way: for a given subset S of the set E, we generate the missing elements $E\backslash S$ with a certain probability distribution $p_{\text{gen}}(E\backslash S|S)$, such that $p_{\text{gen}}(E\backslash S|S)\ |O(S)|$ is now proportional to a proper probability distribution in the configuration space of sets with $|E| = n$ elements. More precisely, given an ensemble E of cardinality n, we define our target equilibrium probability distribution for the Markov chain as

$$p_{\text{eq}}(E) = \frac{\sum_{S\subseteq E} p_{\text{gen}}(E\backslash S|S)\ \lambda_{|S|}\ |O(S)|}{\mathcal{N}_n}, \tag{114}$$

where we have added a weight $\lambda_{|S|} \geq 0$ for later convenience, and $\mathcal{N}_n$ is an unknown normalization factor. With the ensemble probability distribution $p_{\text{eq}}(E)$, it is possible to obtain a Monte Carlo estimator for O_k (see Eq. (113)), for $k \in \{0, 1, \ldots, n\}$

$$O_k = \mathcal{N}_n \left\langle \sum_{S\subseteq E:|S|=k} \frac{p_{\text{gen}}(E\backslash S|S)\ O(S)}{\sum_{S'\subseteq E} p_{\text{gen}}(E\backslash S'|S')\ \lambda_{|S'|}\ |O(S')|} \right\rangle_{p_{\text{eq}}}. \tag{115}$$

The normalization $\mathcal{N}_n$ can be obtained from the zeroth order estimator, which plays the role of an effective normalization sector for the Markov chain

$$\frac{O_0}{O(\emptyset)} = 1 = \mathcal{N}_n \left\langle \frac{p_{\text{gen}}(E|\emptyset)}{\sum_{S'\subseteq E} p_{\text{gen}}(E\backslash S'|S')\ \lambda_{|S'|}\ |O(S')|} \right\rangle_{p_{\text{eq}}}. \tag{116}$$

Detailed balance condition. Our goal is to build a Markov chain of ensembles $E \to E' \to \cdots$, where $|E| = |E'| = n$, that has $p_{\text{eq}}(E)$ as equilibrium probability distribution. We focus

on the following natural update choice for the set E: given the ensemble E, we pick one of the subsets $S \subseteq E$ with probability $\frac{p_{\text{gen}}(E\backslash S|S)\ \lambda_{|S|}\ |O(S)|}{\sum_{S'\subseteq E} p_{\text{gen}}(E\backslash S'|S')\ \lambda_{|S'|}\ |O(S')|}$, and we generate E' with the probability distribution $p_{\text{gen}}(E'\backslash S|S)$. This stochastic process defines the probability of update $p_{\text{update}}(E'|E)$ from the ensemble E to the ensemble E' of the same cardinality ($|E| = |E'| = n$)

$$p_{\text{update}}(E'|E) = \frac{\sum_{S\subseteq E\cap E'} p_{\text{gen}}(E\backslash S|S)\ \lambda_{|S|}\ |O(S)|\ p_{\text{gen}}(E'\backslash S|S)}{\sum_{S'\subseteq E} p_{\text{gen}}(E\backslash S'|S')\ \lambda_{|S'|}\ |O(S')|}. \tag{117}$$

We write the detailed balance condition

$$p_{\text{update}}(E'|E)\ p_{\text{eq}}(E) = p_{\text{update}}(E|E')\ p_{\text{eq}}(E'), \tag{118}$$

and we see that it is verified independently even at the level of each intermediate subset S (hyperdetailed balance).

This update strategy also motivates reasonable choices for λ_k: we choose it in such a way that each order is "chosen" to build the new ensemble a certain fraction of the time. It is particularly important to choose the empty subset $\emptyset$ a non-negligible fraction of the time to have a reasonably well-estimated normalization factor.

Generating sets of configurations. We discuss how to obtain a natural form of $p_{\text{gen}}(E\backslash S|S)$, i.e., the probability of generating the subset $E\backslash S$ starting from the subset S. A natural choice for this distribution can be built starting from the single-vertex probability $p_{\text{gen}}(\{X\}|S)$, which is a probability distribution function that adds a vertex X given the subset of interaction vertices S. A simple and natural choice for $p_{\text{gen}}(\{X\}|S)$ is

$$p_{\text{gen}}(\{X\}|S) = \frac{1}{|S|}\sum_{X_j\in S} p_{\text{gen}}(\{X\}|\{X_j\}), \tag{119}$$

where $p_{\text{gen}}(\{X\}|\{X_j\})$ is the probability distribution of generating the vertex X from the vertex X_j. We also need to define $p_{\text{gen}}(\{X\}|\emptyset)$. Assuming for simplicity that we are considering the grand potential, which is translation invariant, a natural choice can be a uniform probability distribution over spacetime for $p_{\text{gen}}(\{X\}|\emptyset)$.

This formulation has the operational interpretation of uniformly sampling a vertex belonging to the subset S, $X_j \in S$, and generating the vertex X with the probability distribution $p_{\text{gen}}(\{X\}|\{X_j\})$. If we want to generate more than one element, following this stochastic procedure, there is more than one possibility. For instance, to generate the subset $\{X_1, X_2\}$, we can first generate X_1 and then X_2, or in the opposite order. We decide, as a natural choice, to average over all these possibilities. For every subset $S \subseteq \{X_1, \ldots, X_n\}$, we can then write down the probability $p_{\text{gen}}(S'|S)$ of generating the set S', $S' \cap S = \emptyset$, from the set S, as

$$p_{\text{gen}}(S'|S) = \frac{1}{|S'|}\sum_{X\in S'} p_{\text{gen}}(\{X\}|S\cup S'\backslash\{X\})\ p_{\text{gen}}(S'\backslash\{X\}|S), \tag{120}$$

which has a runtime cost of $\mathcal{O}(n\,2^n)$.

5 Summing the expansion: Convergence, singularities and resummation

5.1 Finite radius of convergence and polynomial complexity

It is possible to show that (see e.g. [24]), for all non-zero temperatures, the radius of convergence of the bare expansion is non-zero. More precisely, for quantities such as the grand potential Ω, there exists $R > 0$ such that for $|z| < R$

$$\left| \Omega_{\text{bare}}(z) - \sum_{n=0}^{N} z^n \, \Omega_{\text{bare},n} \right| \leq A_\epsilon \left(\epsilon + \frac{|z|}{R} \right)^{N+1}, \tag{121}$$

for every $\epsilon > 0$. The behavior of the radius of convergence R as a function of β depends on the instabilities of the $U=0$ ground state with respect to small U perturbations: if the non-interacting system is stable at zero temperature for infinitesimal U, which is the case when the system is gapped, then the radius of convergence will be non-zero even at zero temperature. Typically, if a Fermi surface is present, it is unstable at zero temperature towards superconducting, spin, or other ordered states for either $U > 0$ or $U < 0$, or both. This means that the zero-temperature radius of convergence is zero. However, for a fixed U, these Fermi-surface instabilities happen at exponentially low temperature, which means that the inverse of the radius of convergence increases only logarithmically with inverse temperature.
If the radius of convergence is larger than 1, truncating the $z=1$ series at the truncation order n converges exponentially with n. As we have shown that evaluating the coefficient of the series has a cost that increases exponentially with expansion order, the total computational cost $t(\epsilon)$ to obtain a precision of ϵ on a given quantity is polynomial inside the convergence radius (see Ref. [25])

$$t(\epsilon) \sim \epsilon^{-\alpha}, \tag{122}$$

where we have defined $\alpha = \log a / \log R$, and we have assumed that the computational cost to obtain the order n scales as a^n. This result is important as it shows that interacting fermionic quantum matter on the lattice at finite temperature can be simulated with a polynomial-time algorithm, at least in a finite region of the phase diagram. Renormalization allows one to change the region in which this polynomial-time simulation can be achieved by enlarging the radius of convergence. Moreover, using appropriate shifted actions we are able to enter different phases of matter by changing the perturbative starting point.

5.2 Qualitative structure of the singularities and analytic continuation

We now sketch the qualitative structure of the singularities of the bare, non-symmetry-breaking expansion of the two-dimensional Hubbard model, viewed as a function of the complex interaction strength $U \in \mathbb{C}$. This perspective is useful for understanding how the expansion can, in some cases, be analytically continued beyond its radius of convergence.

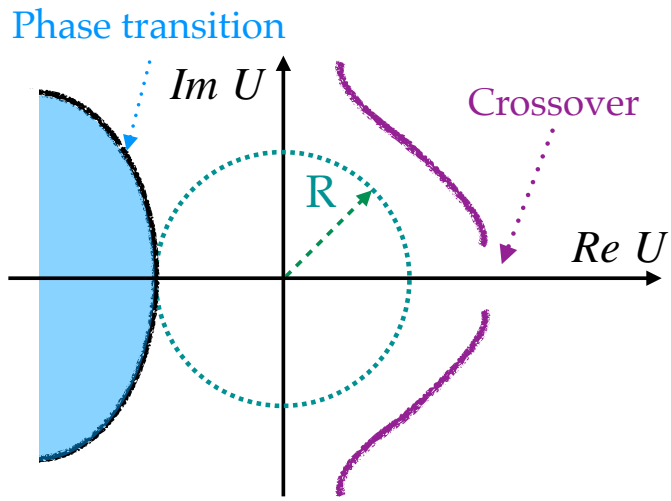

Fig. 5: Qualitative sketch of the complex-U analytic structure of the Hubbard model. *For* $\mathrm{Re}\,U < 0$*, the interaction is attractive, and the system typically becomes unstable toward an* s*-wave superfluid phase. This singularity often sets the radius of convergence of the bare expansion in the doped finite-temperature two-dimensional Hubbard model. The circle* $|U| = R$ *denotes this radius of convergence; for* $\mathrm{Re}\,U > 0$*, however, nothing physical necessarily occurs on this circle. At zero temperature and for repulsive interactions,* $\mathrm{Re}\,U > 0$*, the system is unstable toward antiferromagnetism sufficiently close to half filling. At finite temperature, the corresponding antiferromagnetic singularities do not reach the real axis. As a result, analytic continuation remains possible in principle, while these nearby singularities give rise physically to a crossover regime with strong antiferromagnetic correlations.*

Figure 5 illustrates the typical qualitative structure of the singularities in the complex U plane in the finite-temperature, doped regime of the two-dimensional Hubbard model. For $\mathrm{Re}\,U < 0$, the interaction is attractive. When $\mathrm{Re}\,U$ is sufficiently negative, the system typically becomes an s-wave superfluid. The corresponding singularity often determines the radius of convergence of the expansion, and manifests itself in perturbative coefficients that alternate in sign as a function of expansion order.

The circle $|U| = R$, where R denotes the radius of convergence, is only a mathematical boundary of the Taylor expansion. Nothing special happens on this circle except at the singularity, typically located in the attractive region $\mathrm{Re}\,U < 0$. Therefore, in principle, there is no obstruction to analytically continuing the function beyond this circle in other directions of the complex U plane.

For positive real U, several scenarios are possible. First, there may be no additional singularity beyond the one associated with the attractive side. Second, there may be a singularity on the positive real axis, corresponding to a physical finite-temperature phase transition. In this case, analytic continuation from weak coupling cannot reach the point of interest, since it lies in a different phase of matter. Third, there may be no singularity on the positive real axis, but there may be nearby complex singularities associated with transitions occurring at lower temperature, or possibly at zero temperature. Such singularities do not prevent analytic continuation in principle, but they can generate strong crossover behavior.

Thus, in the first and third scenarios, analytic continuation beyond the radius of convergence is possible in principle and can be attempted using resummation techniques. In practice, however, the difficulty increases as singularities approach the positive real axis. Since one usually has access only to a finite number of expansion orders, typically of order $\mathcal{O}(10)$, there is a practical limit to the regions of the phase diagram, in temperature and interaction strength, that can be reliably reached by resummation.

6 Conclusions

We have introduced Diagrammatic Monte Carlo as a way to exchange the exponential scaling of the many-body system with a series summation problem. Focusing on the Hubbard model, we have discussed the choice of the diagrammatic expansion, how to efficiently evaluate Feynman diagrams, and how to sum the resulting series based on the analytic properties of the expansion function. We have shown that recent algorithms for summing all Feynman diagrams make it possible to achieve a polynomial-time solution of the many-electron problem in some parameter regimes. This has made it possible to characterize the finite-temperature regime of the two-dimensional doped Hubbard model, notably the pseudogap and the magnetic crossovers, in a controlled way. Future work in the Hubbard model should be devoted to extending the range of applicability of the technique with the help of new renormalization schemes and strong-coupling descriptions, and to entering broken-symmetry phases including stripes and the long-conjectured d-wave superconducting state.

References

[1] J. Hubbard, Proc. R. Soc. Lond. A **276**, 238 (1963)

[2] D.P. Arovas, E. Berg, S.A. Kivelson, and S. Raghu,
Annu. Rev. Condens. Matter Phys. **13**, 239 (2022)

[3] M. Qin, T. Schäfer, S. Andergassen, P. Corboz, and E. Gull,
Annu. Rev. Condens. Matter Phys. **13**, 275 (2022)

[4] R. Rossi, F. Werner, N. Prokof'ev, and B. Svistunov, Phys. Rev. B **93**, 161102(R) (2016)

[5] R. Rossi, F. Šimkovic, and M. Ferrero, EPL **132**, 11001 (2020)

[6] G. Spada, R. Rossi, F. Šimkovic, R. Garioud, M. Ferrero, K. Van Houcke, and F. Werner,
arXiv:2103.12038

[7] R. Garioud, F. Šimkovic, R. Rossi, G. Spada, T. Schäfer, F. Werner, and M. Ferrero,
Phys. Rev. Lett. **132**, 246505 (2024)

[8] E. Kozik, M. Ferrero, and A. Georges, Phys. Rev. Lett. **114**, 156402 (2015)

[9] R. Rossi and F. Werner, J. Phys. A: Math. Theor. **48**, 485202 (2015)

[10] N.V. Prokof'ev and B.V. Svistunov, Phys. Rev. Lett. **99**, 250201 (2007)

[11] K. Van Houcke, E. Kozik, N. Prokof'ev, and B. Svistunov, Phys. Procedia **6**, 95 (2010)

[12] E. Kozik, K. Van Houcke, E. Gull, L. Pollet, N. Prokof'ev, B. Svistunov, and M. Troyer,
EPL **90**, 10004 (2010)

[13] N. Prokof'ev: *Diagrammatic Monte Carlo*, in E. Pavarini, E. Koch, and S. Zhang (eds.):
Many-Body Methods for Real Materials, Modeling and Simulation Vol. 9
(Forschungszentrum Jülich, 2019)

[14] A.N. Rubtsov, V.V. Savkin, and A.I. Lichtenstein, Phys. Rev. B **72**, 035122 (2005)

[15] E. Gull, A.J. Millis, A.I. Lichtenstein, A.N. Rubtsov, M. Troyer, and P. Werner,
Rev. Mod. Phys. **83**, 349 (2011)

[16] R.M. Karp, in R.E. Miller and J.W. Thatcher (eds.):
Complexity of Computer Computations (Plenum, New York, 1972), pp. 85–103

[17] M. Held and R.M. Karp, J. Soc. Indust. Appl. Math. **10**, 196 (1962)

[18] R. Bellman, J. ACM **9**, 61 (1962)

[19] R. Rossi, Phys. Rev. Lett. **119**, 045701 (2017)

[20] A. Björklund, T. Husfeldt, P. Kaski, and M. Koivisto, in *Proceedings of the 39th Annual ACM Symposium on Theory of Computing* (STOC 2007), pp. 67–74

[21] F. Šimkovic, R. Rossi, A. Georges, and M. Ferrero, Science **385**, ade9194 (2024)

[22] E. Kozik, Nat. Commun. **15**, 7916 (2024)

[23] F. Šimkovic and R. Rossi, arXiv:2102.05613

[24] G. Benfatto, A. Giuliani, and V. Mastropietro, Ann. Henri Poincaré **7**, 809 (2006)

[25] R. Rossi, N. Prokof'ev, B. Svistunov, K. Van Houcke, and F. Werner, EPL **118**, 10004 (2017)